Shear response of Σ3{112} twin boundaries in face-centered-cubic metals

J. Wang,[1,*] A. Misra,[2] and J. P. Hirth[2]

[1]*Materials Science & Technology Division, MST-8, Los Alamos National Laboratory, Los Alamos, New Mexico 87545, USA*

[2]*Materials Physics & Applications Division, CINT, Los Alamos National Laboratory, Los Alamos, New Mexico 87545, USA*

(Received 14 October 2010; published 18 February 2011)

Molecular statics and dynamics simulations were used to study the mechanisms of sliding and migration of Σ3{112} incoherent twin boundaries (ITBs) under applied shear acting in the boundary in the face-centered-cubic (fcc) metals, Ag, Cu, Pd, and Al, of varying stacking fault energies. These studies revealed that (i) ITBs can dissociate into two phase boundaries (PBs), bounding the hexagonal 9*R* phase, that contain different arrays of partial dislocations; (ii) the separation distance between the two PBs scales inversely with increasing stacking fault energy; (iii) for fcc metals with low stacking fault energy, one of the two PBs migrates through the collective glide of partials, referred to as the phase-boundary-migration (PBM) mechanism; (iv) for metals with high stacking energy, ITBs experience a coupled motion (migration and sliding) through the glide of interface disconnections, referred to as the interface-disconnection-glide (IDG) mechanism.

DOI: 10.1103/PhysRevB.83.064106 PACS number(s): 61.72.Mm

I. INTRODUCTION

Σ3{112} incoherent twin boundaries (ITBs) have recently attracted considerable attention, since they often form during the formation of growth twins[1–5] and they play a crucial role in the mechanical deformation of nanotwinned metals, in particular, when the height of ITBs is a few nanometers.[6–9]

In epitaxial nanotwinned Cu, growth twin lamellae have long Σ3{111} coherent twin boundaries (CTBs) normal to the growth direction, truncated by short Σ3{112} ITBs.[5,7,8] Nanotwinned Cu has been shown to exhibit an unusual combination of ultrahigh strength, high electrical conductivity, high ductility, high thermal stability, and fatigue resistance.[10–18] Lu and co-workers[10–12] showed that the introduction of coherent growth nanotwins, typically tens of nanometers in thickness, in ultrafine-grained copper (with a grain size of several hundred nanometers) leads to an unusual combination of ultrahigh strength (1 GPa) and high ductility (14% elongation to failure). Zhang and co-workers[13,14] found that austenitic 330 stainless-steel (330 SS) films containing nanoscale coherent growth twins have an order of magnitude higher mechanical strength than the bulk, that sputter-deposited nt Cu foils[6] have the high flow stress of 1.2 GPa, and that comparable high strengths are achieved in epitaxial nanotwin (nt) Cu films.[5] This unusual high strength originates from Σ3(111) CTBs, with an average twin spacing of a few nm, which act as strong barriers for slip transfer of single dislocations.[16–21] ITBs have been studied with high-resolution transmission electron microscopy (HRTEM)[1–4,7] and molecular statics (MS) simulations.[7,8] The results show that ITBs can be represented as an array of Shockley partial dislocations on every {111} plane.[7] The roles of ITBs in mechanical deformation have been studied using molecular dynamics (MD).[22,23]

A critical issue is the stability of growth nanotwins, i.e., whether coherent twin boundary motion is reversible during deformation. We recently observed that very thin twins (less than 2 nm thick) annihilate during rolling of nt Cu foils, and ascribed the driving force for the annihilation to an attractive twin-twin interaction.[24] However, these *ex situ* studies may not reveal how detwinning occurs and what kinetic processes are involved during the annihilation of coherent twin boundaries. Using *in situ* nanoindentation in a TEM,[8–10] we observed the rapid migration of ITBs (causing the annihilation of CTBs) in epitaxial nt Cu films. In parallel, we showed, by topological analysis and MD simulations, that the detwinning process occurs by migration of ITBs, because transformation disconnections (TDs) in ITBs are glissile.[8] The results imply that detwinning becomes the dominant deformation mechanism, at low plastic strains, for structures with growth twins on the order of a few nanometers thick. Hence detwinning in polycrystalline nanotwinned Cu could be a dominant deformation mechanism when twins are a few nanometers thick, and hence result in softening.[11,25] When growth twins are thicker, statistically, the chance of the interaction of lattice dislocation with ITBs is greater. *In situ* TEM observations show that such ITBs can be pinned because of the dislocation-ITB interaction, resulting in a hardening effect.[10] The unresolved issue in the earlier work is the stress-induced-migration resistance of Σ3{112} ITBs in terms of the defect structure of the ITB and the stacking fault energy of the metal.

In this work, we have used MD simulations to study the shear response of Σ3{112} ITBs in fcc metals with a range of stacking fault energies: Ag (26 mJ/m^2), Cu (45 mJ/m^2), Pd (98 mJ/m^2), and Al (146 mJ/m^2). This paper is organized as follows. In Sec. II we briefly describe the dislocation structure of ITBs using a topological model, and address the influence of stacking fault energies on the atomic structure of ITBs using MS. In Sec. III, we report on the sliding and migration mechanisms of ITBs under applied shear parallel to ITBs. Finally, we present our conclusions in Sec. IV.

II. ATOMIC STRUCTURES OF Σ3{112} ITBs

We first examine the influence of stacking fault energy on the atomic structure of Σ3{112} ITBs. To understand the defect structure of ITBs, we construct the ⟨110⟩Σ3{112}‖{112} dichromatic pattern, with a vertical ITB, shown in Fig. 1. The zone axis is parallel to the [$\bar{1}$10] direction pointing out of the figure. The solid symbols represent atoms in grain α and the empty symbols represent atoms in grain β. They adopt the twin orientation relationship. Since {110} planes with a normal direction along the z axis have a repeatable stacking sequence ...*ababab*..., we present atoms in the *a*

 ©2011 American Physical Society

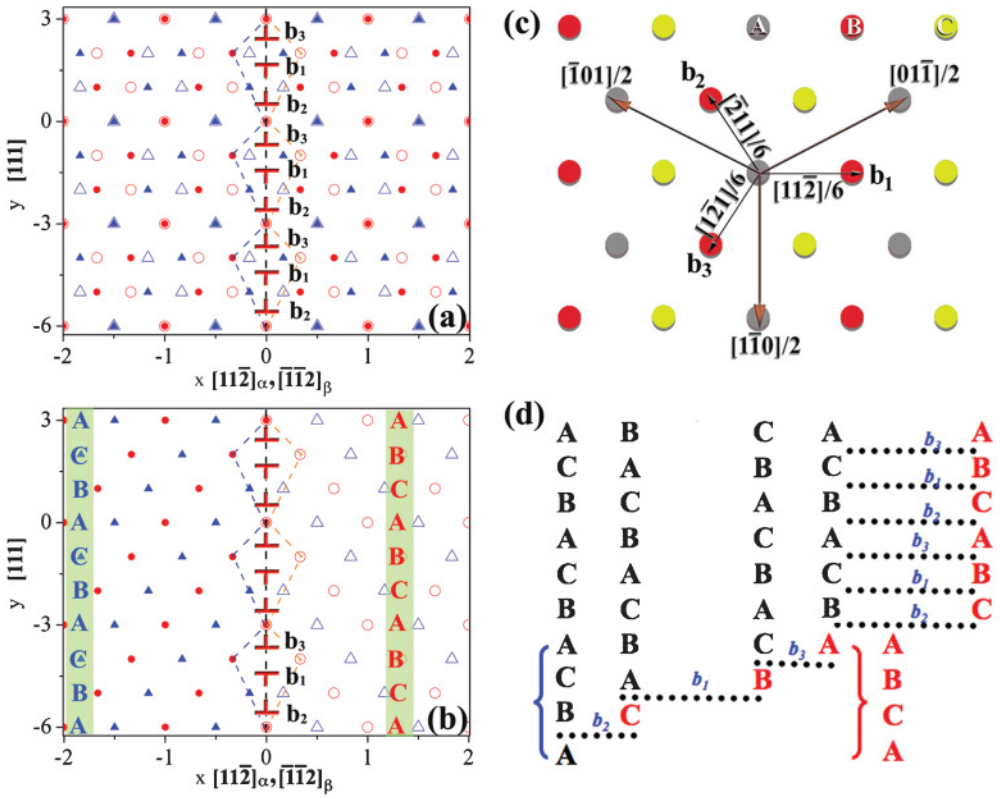

FIG. 1. (Color online) Dichromatic pattern of a [110]Σ3{112}‖{112} twin boundary showing the atomic structure of the boundary: (a) Dichromatic pattern of an ITB containing a set of partial dislocations on every (111) plane with a repetitive sequence b_2:b_1:b_3, and (b) the equivalent bicrystal structure of an ITB. The dashed lines outline the boundary atoms belonging to two grains. (c) Plan view of (111) plane stacking and three partials. b_1 is a pure edge dislocation, b_2 and b_3 are mixed partial dislocations with opposite sign screw components. (d) Schematic illustration of the glide of the three partials to create a twin. The length units are $|\frac{a}{2}[112]|$ for the x axis and $|\frac{a}{3}[111]|$ for the y axis. The solid symbols represent atoms in grain α and the empty symbols represent atoms in grain β. The repeatable pattern with a unit involving three {111} planes is delineated by solid lines. The sense vector $\boldsymbol{\xi}$ points out of the figure in this and the following figures. The black symbols in (d) represent the initial (111) plane stacking in a perfect crystal and the red symbols represent the final (111) plane stacking in the twinned crystal.

plane as circles and atoms in the b plane as triangles. The left crystal is designated α and is presented by solid symbols, and the right one, β, is presented by empty symbols. This geometric model reveals a repeatable unit within the interface [as outlined by dashed lines in Figs. 1(a) and 1(b)] involving three adjacent {111} planes. For either deformation or growth twins, these units can be represented as an array of Shockley partial dislocations.[26–28] For deformation twins created during mechanical deformation, the partials usually have the same Burgers vector so that the Peach-Koehler glide forces on the partials have the same sign and they move along the same direction.[26,27] But this is not necessary for growth twins, such as those in sputtered epitaxial nt Cu films.[7,8] Σ3{112} ITBs observed in experiments on growth twins[5–7] can be represented as a set of partial dislocations on every {111} plane with a repeatable sequence b_1:b_2:b_3, as shown in Fig. 1.[7] The Burgers vector b_1 is equal to $\frac{1}{6}[11\bar{2}]$, a pure edge partial dislocation; b_2 and b_3 are equal to $\frac{1}{6}[\bar{2}11]$ and $\frac{1}{6}[1\bar{2}1]$, respectively, both of which are mixed partial dislocations with opposite sign screw components [Fig. 1(c)]. The sum of the Burgers vectors in one triple unit equals zero. The formation of a twin by the successive motion of these three partials is schematically depicted in Fig. 1(d).

In the absence of external stress, the dissociation of partial dislocations in ITBs can occur spontaneously because of a reduction in core energy.[29] To determine the width of the dissociated region and identify how they dissociate, molecular statics calculations are performed for ITBs in fcc metals under zero applied stress. We created ITBs from a perfect crystal by gliding a set of partial dislocations on every (111) plane with an order of $\boldsymbol{b}_2$:$\boldsymbol{b}_1$:$\boldsymbol{b}_3$. The coordinate system adopted for the initial crystal is x axis along $[11\bar{2}]_\alpha$, y axis along $[111]_\alpha$, and z axis along $[\bar{1}10]_\alpha$: for the twin, the x and z axes have opposite signs. The model is periodic along both the z axis and the y axis, as shown in Fig. 2. The interface plane is the y-z plane. Embedded atom method (EAM) potentials[30] are adopted, Ag,[31] Cu,[32] Pd,[31] and Al.[33] These potentials have produced reliable results in studies of the energetics and kinetics of surfaces,[34,35] defects and interfaces,[36,37] and crystal growth.[38,39] The dimension of the computation cell in the x direction is 60 periods along $\frac{1}{2}\langle 112\rangle$ for both grains, and in z the direction, six periods along $\frac{1}{2}\langle 110\rangle$. The dimension in the y direction is six periods along [111]. Relaxation of the bicrystal model is accomplished by the quenching molecular dynamics method.[40,41] During relaxation, a flexible boundary condition is imposed at twice the potential cutoff thickness

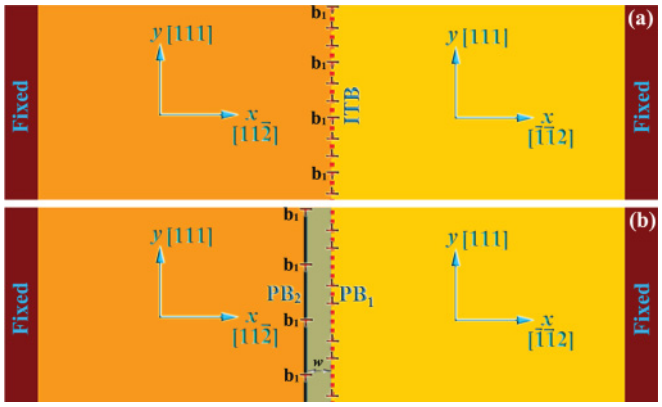

FIG. 2. (Color online) Simulation setup for MD: (a) initial ITB created through the glide of partials on every (111) plane, and (b) schematic illustration of the dissociation of partials in the initial ITB, resulting in two phase boundaries comprising different arrays of partials.

in the x direction for both matrix and twinned grains, so that the two grains are able to translate in all three directions, but not able to rotate.[40] All atom positions are allowed to relax fully and independently until the maximum force acting on any atom does not exceed 5 pN. The net forces, acting parallel and perpendicular to the interface, drive the translations.[40,42]

The fully relaxed atomic structures of the ITBs are shown in Fig. 3, indicating the dissociation of sets of partials in the ITBs. Disregistry analysis[40] is then performed across three different (111) planes. The result (in Fig. 4) shows that the

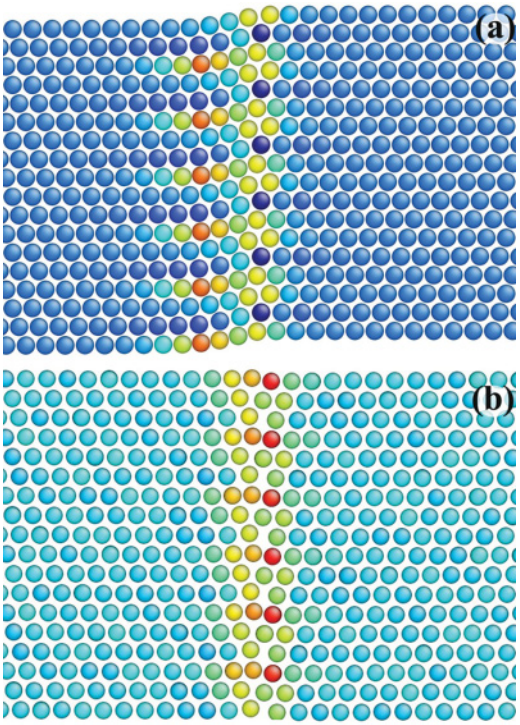

FIG. 3. (Color online) Relaxed atomic structures of Σ3{112} IGBs under zero applied stress, showing (a) atomic structure in Cu, and (b) atomic structure in Al. Different atom colors represent different excess potential energies.

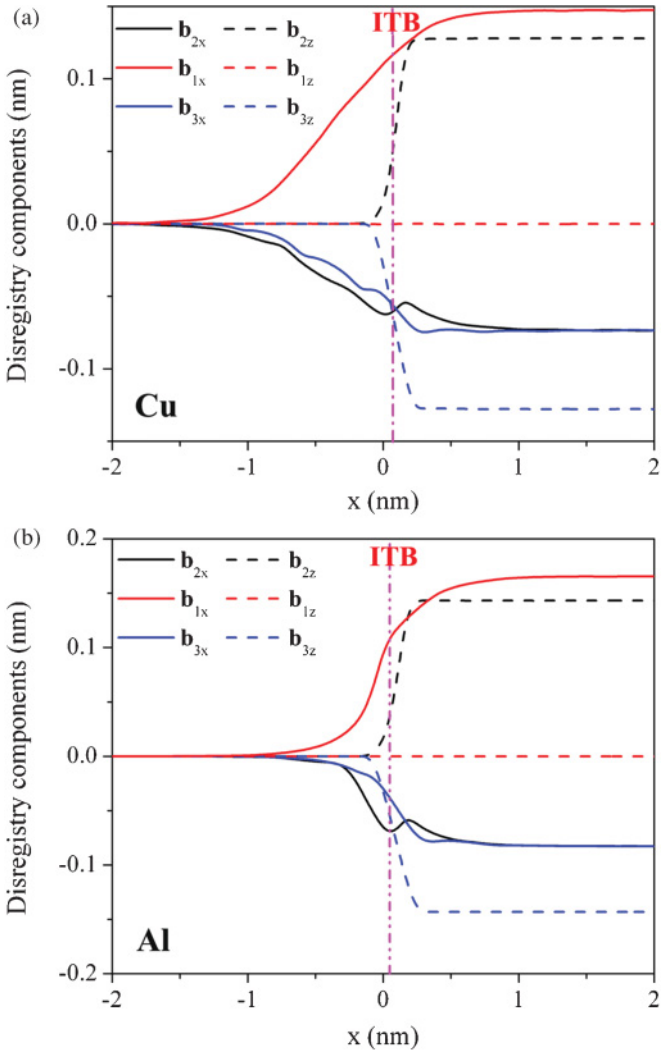

FIG. 4. (Color online) Disregistry plots of the three partial dislocations in an ITB: (a) in Cu and (b) in Al. From this plot, the size of the dissociation region can be determined as half of the magnitude of the x component of Burgers vector of partial $\boldsymbol{b}_1$. The results are summarized in Table I.

dissociation is achieved by the emission of one set of partials away from the initial compact ITBs. Corresponding to this dissociation, a 9R phase forms between the two resulting partial dislocation tilt walls, as shown in Fig. 2. Analogous to the discussion in Sec. 10-2 of Ref. 26, this dissociation changes the (111) plane stacking to conform to 9R. The normal fcc stacking is . . .***ABCABCAB***. . .. The passage of any one among the three partials $\boldsymbol{b}_1$, $\boldsymbol{b}_2$, or $\boldsymbol{b}_3$ shifts the sequence in the manner $\boldsymbol{A} \rightarrow \boldsymbol{B} \rightarrow \boldsymbol{C} \rightarrow \boldsymbol{A}$. This creates a 9$R$ structure with the stacking sequence . . .***BCBCACABA***. . .. Since the partials $\boldsymbol{b}_2$ and $\boldsymbol{b}_3$ attract each other because of their opposite sign screw components, the emitted partial is $\boldsymbol{b}_1$, as shown in Fig. 2(b). The 9R phase is not thermodynamically stable in this system in the absence of defects. The 9R phase forms because the dissociation is driven by the accompanying decrease in core energy or, in the presence of stress, by the associated Peach-Koehler force—an interesting and seldom encountered category of phase formation.

TABLE I. The influence of stacking fault energy on the atomic structure of ITBs.

Materials	γ_{SF} (mJ/m^2)	E_{ITB} (mJ/m^2)	w (nm)	R_w
Ag	26	397	0.97	3.31
Cu	45	590	0.80	3.13
Pd	98	570	0.50	1.81
Al	165	357	0.30	1.04

The width of the dissociated region w is determined according to the disregistry plot, as shown in Fig. 4. Excess potential energies for the ITBs in Ag, Cu, Pd, and Al are 397, 590, 570, and 357 mJ/m^2, respectively. The widths of the ITBs in Ag, Cu, Pd, and Al are 0.97, 0.80, 0.50, and 0.30 nm, respectively. To eliminate the effect of the lattice parameter in describing the width, a dimensionless factor R_w is defined with the form of $R_w = w/|b_p|$. Here $|b_p|$ is the length of the partial dislocation Burgers vector, $\frac{a}{6}\langle 112\rangle$. Correspondingly, the dimensionless factor R_w is equal to 3.31, 3.13, 1.81, and 1.04 for ITBs in Ag, Cu, Pd, and Al, respectively. The results, summarized in Table I, show that (i) the dimensionless factor R_w, corresponding to the width of the dissociated region, decreases as the stacking fault energy increases; (ii) for fcc metals with high stacking fault energy, the dimensionless factor R_w is close to 1. For instance, the factor is approximately equal to 1 in Al, suggesting that $\Sigma 3\{112\}$ ITBs in Al do not significantly dissociate since the spacing is approximately equal to a single dislocation core.

III. SHEAR RESPONSE OF $\Sigma 3\{112\}$ ITBs

A. Theoretical models

Molecular statics simulations have predicted the dissociation of ITBs of the above type in fcc metals with low stacking fault energies, but no obvious dissociation for fcc metals with high stacking fault energy. Under shear stresses, partial dislocations $\boldsymbol{b}_1$ are expected to glide along one direction and the two partial dislocations $\boldsymbol{b}_2$ and $\boldsymbol{b}_3$ in the opposite direction if the Peach-Koehler glide force on them exceeds the Peierls force. As a result, the 9R phase can propagate. Correspondingly, we refer to this mechanical response process as the phase-boundary-migration mechanism (PBM).

The dissociation, however, could be difficult for fcc metals with high stacking fault energy even under applied stress. The PBM mechanism may not operate for these materials. The other mechanism, the so-called coupled grain-boundary (GB) motion, is more suitable in describing shear behavior of such ITBs.

Many grain boundaries have the property that their normal motion (migration) requires a simultaneous relative translation of the adjacent grains parallel to the GB plane (sliding).[43–45] This motion, in turn, produces shear deformation of the material swept by the boundary. The coupling effect is characterized by a factor β equal to the ratio of the tangential grain translation velocity to the accompanying normal GB displacement velocity. Such coupled GB motion has been verified extensively in atomistic simulations.[44–46] Stress-induced GB motion has been observed in experiments on bicrystals in both metals[47–50] and ceramic materials.[51] To identify this kinetic process in ITBs, we employed the topological model of interface defects,[52,53] wherein the motion of an interface disconnection can be quantified in terms of a disconnection, characterized by its Burgers vector $\boldsymbol{b}$, step height h, and the densities of each atomic species in the adjacent crystals.[52] Here h is represented as nd, where d is the interplanar repeat distance, and characterized by n. The conservative motion of a disconnection along an interface causes atoms in a specific volume of one of the crystals to be relocated to sites in a corresponding volume of the other. Eligible interfaces are those where the atoms in corresponding volumes of the two crystals have equal area density when projected onto the interface plane. An interface disconnection is identified in a dichromatic complex constructed as the superposition of the matrix and twinned atomic crystal structures, with a common incoherent twin plane identified and the structures defined by a set of structure translation vectors **t** for both structures. An interface disconnection is then selected with a given step height and a Burgers vector that is the difference between the **t** vectors. The movement of atoms as twinning disconnection (TD) moves can be described as the translation of the CTB by h, together with a shear produced by the Burgers vector $\boldsymbol{b}$. In general there also may be a local series of shuffles.[54,55]

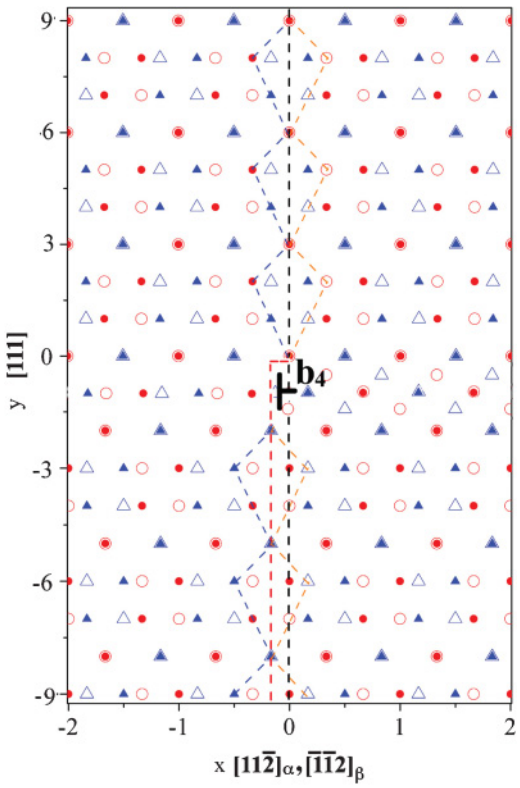

FIG. 5. (Color online) Interface disconnection glide mechanism of ITBs. Dichromatic pattern of a $[110]\Sigma 3\{112\}\|\{112\}$ twin boundary showing the atomic structure after the lower part of grain β (symbolized with empty circles and triangles) shifts upward with a magnitude of $\frac{2}{3}[111]$. The black dashed line indicates the location of the initial ITB and the red dashed line indicates the final location of the ITB. The solid symbols represent atoms in grain α and the empty symbols represent atoms in grain β. The length units are $|\frac{a}{2}[112]|$ for the x axis and $|\frac{a}{3}[111]|$ for the y axis.

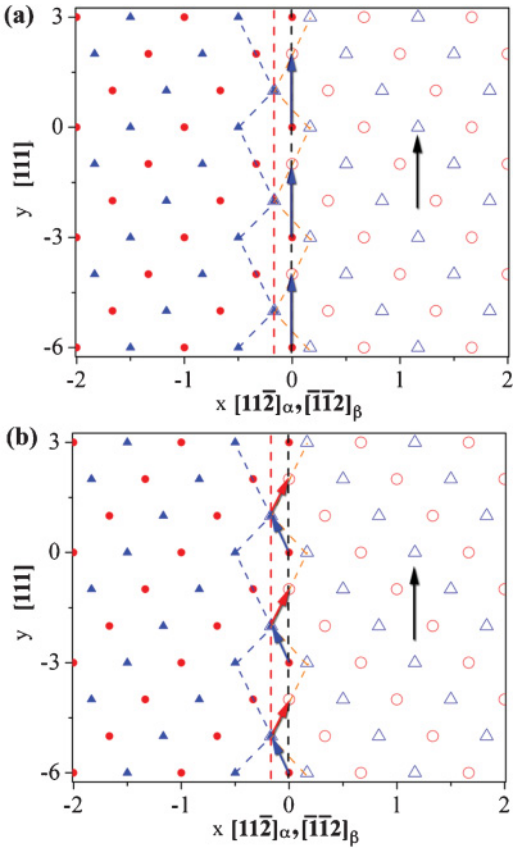

FIG. 6. (Color online) Possible kinetics processes involved in the glide of interface disconnection. (a) Red solid spheres move upward ($\frac{2}{3}$[111]) to red empty circles; (b) red solid spheres move to blue triangles, and blue triangles move to red empty circles, corresponding to a synchroshear shuffle mechanism. The length units are $|\frac{a}{2}[112]|$ for the x axis and $|\frac{a}{3}[111]|$ for the y axis.

Analysis of the dichromatic complex in Fig. 1 reveals that the appropriate unit transformation disconnection in this case is that in Fig. 5. The step height is $n = 1$ and $d = |1/6\langle 112\rangle|$, and the Burgers vector is $b_4 = \frac{2}{3}\langle 111\rangle$. After the glide of the disconnection, all blue symbols move upwards two (111) interplanar distances relative to the reference in Fig. 1(a). The ITB is outlined with dashed lines in Fig. 5. Comparing atomic structures in the top part (initial GB) with the low part (new GB), one sees that TD motion causes the red solid spheres (under the black dashed line and belonging to the initial ITB) to move to the red circles (under the black dashed line and belonging to the grain β). There are two possible pathways corresponding to atom movements accompanying disconnection motion, as shown in Fig. 6. (i) Atoms experience the same displacements as other atoms in grain β, i.e., $u = \frac{2\sqrt{3}}{3}a$, where a is the lattice parameter along the shear direction [Fig. 6(a)]; and (ii) atoms in the initial ITB and the final ITB experience a collective synchroshear shuffle[56] by exchanging their positions as shown in Fig. 6(b); the corresponding displacement magnitude is $u = \frac{\sqrt{11}}{2\sqrt{6}}a$. No matter which kinetic process operates, ITBs can move in a coupling fashion through the glide of interface disconnection. The factor β then can be calculated as $\beta = |\frac{2}{3}[111]|/|\frac{1}{6}[112]| = 2\sqrt{2}$. Correspondingly, we refer to this mechanism as the interface-disconnection-glide mechanism (IDG).

B. Molecular dynamics simulations

In order to verify the two possible mechanisms, PBM (corresponding to the growth of the 9R phase) and IDG (the coupling motion of ITB as a result of the glide of interface disconnection), as well as to identify the details of the disconnection displacements for the IDG mechanism, we performed atomistic simulations for ITBs under shear stresses τ_{xy} acting in the interface plane.

With the ITB subjected to a shear stress τ_{xy}, molecular dynamics calculations were performed at a constant temperature of 5 K. The bicrystal model with the ITB is homogeneously, gradually sheared by the application of displacement gradients to the simulation cell, with one nonzero term, $\partial u_y/\partial x$, applied in an increment of 0.001 at every loading step. Here, u_y is the displacement along the y direction. After the displacement gradient increments are applied, MD was applied for 20 ps, followed by quenching until the maximum force acting on any atom in the system is less than 5 pN.[40,41] The results are plotted in Fig. 7, showing the shear stress as a function of the applied shear strain. There are two sets of typical stress-strain curves: type I gradually increases then becomes flat, and type II linearly increases then quickly drops, with increasing applied strain. From the two sets of stress-strain curves, we identify the two motion mechanisms, i.e., PBM and IDG, with respect to the stacking fault energies. The results show that the motion of ITBs in fcc metals is dependent on the stacking fault energy; IDG is likely for fcc metals with high stacking fault energy and PBM is likely for fcc metals with low stacking fault energy.

We first discuss type I, corresponding to the PBM mechanism. Taking Cu as an example, Fig. 8(a) shows atomic structures with the extended 9R phase, and Fig. 8(b) shows the growth of 9R phase as a function of the applied shear strain and the stress-strain response. Five important aspects are revealed. (i) The width of the 9R phase region and the shear stresses on the bicrystal both increase nonlinearly with the accumulated displacement gradient component. This nonlinear behavior

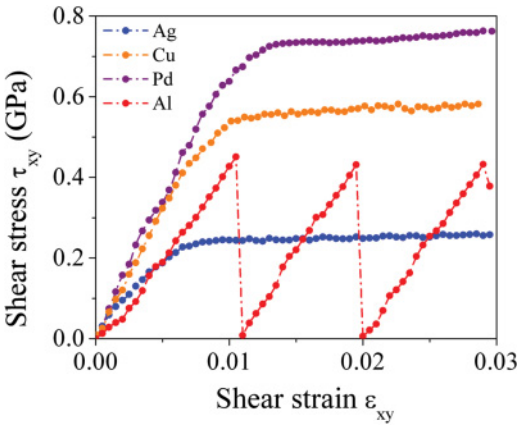

FIG. 7. (Color online) Mechanical response of ITBs in Ag, Cu, Pd, and Al when the bicrystal model is subjected to shear stresses acting in the ITB plane, revealing two typical stress-strain behaviors that correspond to the two different motion mechanisms.

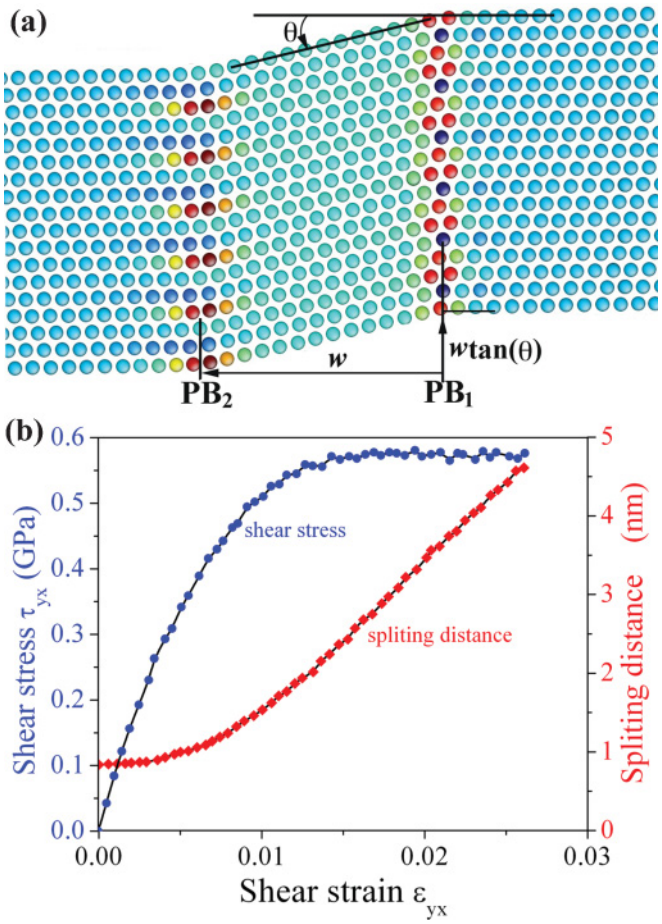

FIG. 8. (Color online) Phase-boundary-migration (PBM) mechanism verified in Cu by MD simulation. (a) Atomic structure of the dissociated $\Sigma 3\{112\}$ ITBs in Cu under applied shear stress, showing the migration of PB_2 through a collective glide of partials $\boldsymbol{b}_1$, and (b) shear stress and dissociation distance of the emitted partial dislocation from the initial boundary as a function of applied displacement gradients. Atoms are colored by their excess potential energies. The 9*R* phase is the region between the two PBs. The angle θ is 13.0°.

is mainly ascribed to the nonlinear interaction forces of the interacting sets of dislocations (see Sec. 19-5 in Ref. 26). (ii) The width of the 9*R* phase region increases linearly and the shear stresses remain constant with the accumulated ε_{yx} when its value exceeds 0.011. This linear response corresponds to the applied force balancing the constant attractive force γ_{SF} acting on the partial dislocation $\boldsymbol{b}_1$. The transition from nonlinear to linear originates from two factors. The nonlinear dislocation interactions reduce to linear interactions for separations $w >\sim 1$ nm.[26] Similarly, the stacking fault energy is a nonlinear decreasing function of w, approaching a constant value when $w >\sim 1$ nm.[26] (iii) The other two partial dislocations b_2 and b_3 remain at their initial positions during the growth of the 9*R* phase. This observation implies that the summed Peierls barrier for the glide of the two paired partial dislocations b_2 and b_3 is higher than that for the partial dislocation b_1. (iv) As a result of the emission of partial dislocations on every third (111) plane, the separated boundaries have tilt components and the 9*R* phase is locally rotated relative to the bounding fcc phases by $+/-$ 13.0°. This angle is approximately equal to the theoretical estimate of 13.28° from the dislocation-based tilt wall model with a partial dislocation b_1 on every third (111) plane.[57–59] (v) Corresponding to the tilt of the 9*R* phase relative to grain α, the grain α achieves a relative displacement parallel to the interface plane. The relative displacement corresponds to a shear deformation occurring in grain α and can be calculated as a function of tilt angle and the width of the 9*R* phase region, i.e., $w\tan(\theta)$. Thus the factor β is equal to $\tan(\theta)$ as a result of $w\tan(\theta)/w$ corresponding to the ratio of tangential displacement with respect to the normal displacement in association with the migration of PB_2.

Type II corresponds to the IDG mechanism. Taking Al as an example, Fig. 9 shows atomic structures of ITBs (a) at peak stress and (b) after the stresses drop. The result shows that atoms in grain α move upward by two (111) interplanar spacings, corresponding to the expected Burgers vector of $b_4 = \frac{2}{3}[111]$. Figure 10 shows atom movement after the stress drop, and reveals that (i) ITBs migrate from the right to the left with the magnitude of $h = |\frac{1}{6}\langle 112\rangle|$, or $n = 1$; (ii) atoms belonging to the initial ITB and the final ITB experience shuffling corresponding to the second theoretical possibility, Fig. 6(b); and (iii) atoms on the right of the initial ITB experience a simple shear displacement with the magnitude of $\frac{2}{3}[111]$. Thus the factor β is equal to $2\sqrt{2}$ corresponding to the ratio of tangential displacement with respect to the

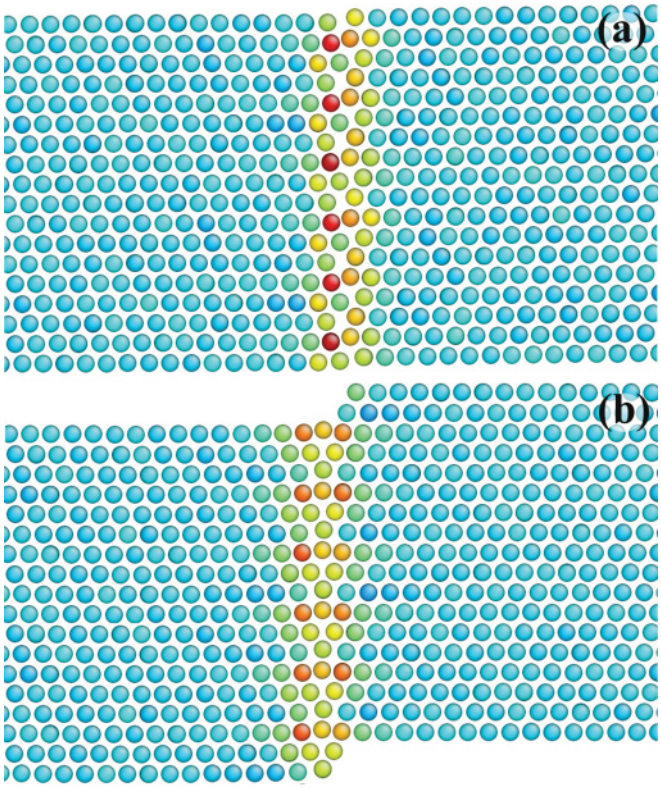

FIG. 9. (Color online) Interface disconnection glide mechanism verified in Al by MD simulation. (a) Atomic structure of an ITB before the glide of one disconnection, and (b) atomic structure of the ITB after the glide of one disconnection. Atoms are colored by their excess potential energies.

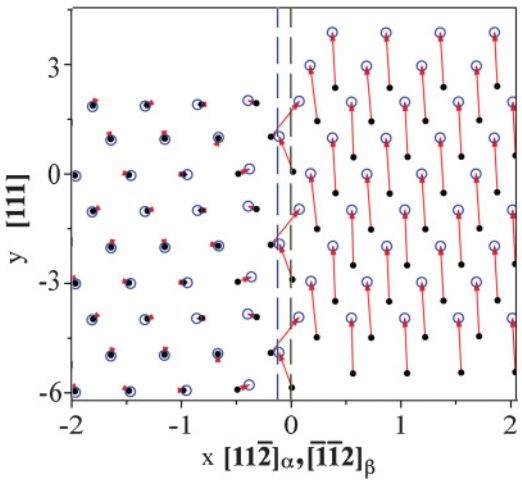

FIG. 10. (Color online) Vector plot shows atom displacements in association with the glide of one disconnection. The length units are $|\frac{a}{2}[112]|$ for the x axis and $|\frac{a}{3}[111]|$ for the y axis.

normal displacement in association with the glide of interface disconnection.

Temperature could affect shear response of $S3\{112\}$ ITBs in terms of mobility because the formation and motion of kinks and/or interface disconnections are easier at elevated temperatures.[8] However, it must be pointed out that the separation distance of two PBs at zero applied stress is independent of temperature, because stacking fault energy is insensitive to temperature.[7] Corresponding to the PBM mechanism under applied shear stress at room temperature, the partial dislocation b_1 in PB2 is initially more mobile than the other two partial dislocations in PB1 because of a lower Peierls barrier. For the near equilibrium case, a slight increase in stress would move the partial dislocation b_1 to the one side, and move the paired partials b_2 and b_3 to the other side when the Peierls stress is weak. For the first scenario, an increased stress is required for the partial dislocation b_1 to overcome the interaction force, but the latter drops as it moves, tending to produce breakaway at constant stress. However, locally the plastic strain associated with the motion of the partials should produce a load drop, tending to arrest the motion. Then the paired partials would have γ_{SF} plus the interaction force pulling them and a decreased applied force acting on the paired partials so they could move to approach the b_1 partial until again reaching the equilibrium spacing. The process could repeat, resulting in the migration of ITBs in the direction favored by the applied force acting on the b_1 partials. Locally, the situation would represent a stop/start displacement situation with some waiting time.[8] Corresponding to the IDG mechanism, the formation of interface disconnection is a thermally activated process. Therefore the coupling motion of ITBs under applied shear stress at room temperature becomes easier.

IV. CONCLUSIONS

We studied the shear response of ITBs in fcc metals using topological analysis and atomistic simulations. The topological analysis reveals the nature of the ITBs in terms of dislocation structures, and further possible motion mechanisms of ITBs: phase-boundary-migration mechanisms and interface-disconnection-glide mechanisms. MS/MD simulations examined the predictions from topological analysis and revealed kinetic processes in association with the two mechanisms. The results show that the motion mechanisms are related to atomic structures of ITBs, in turn, affected by stacking fault energy. The key conclusions are summarized as follows.

(1) ITBs can dissociate into two phase boundaries, bounding a 9R phase, that contain different arrays and numbers of Shockley partial dislocations.

(2) The separation distance between the two phase boundaries scales inversely with the stacking fault formation energy.

(3) For fcc metals with low stacking fault energy, one of the two phase boundaries migrates under shear stress parallel to ITBs, corresponding to the growth of the 9R phase.

(4) For fcc metals with high stacking energy, ITBs experience a coupled motion (sliding and migration) through the glide of interface disconnections with Burgers vectors $\frac{2}{3}[111]$ and unit step height.

(5) In addition to the shear accompanying the glide of the interface disconnections, there are local shuffles.

ACKNOWLEDGMENTS

This work was supported by the US Department of Energy, Office of Science, Office of Basic Energy Sciences. The authors acknowledge fruitful collaborations with R.G. Hoagland, N. Li, and X. Zhang.

*Author to whom correspondence should be addressed. wangj6@lanl.gov

[1]D. Hofmann and F. Ernst, Ultramicroscopy **53**, 205 (1994).
[2]J. D. Rittner, D. N. Seidman, and K.L. Merkle, Phys. Rev. B **53**, R4241 (1996).
[3]G. Lucadamo and D. L. Medlin, Science **300**, 1272 (2003).
[4]D. L. Medlin, G. H. Campbell, and C. B. Carter, Acta Mater. **46**, 5135 (1998).
[5]O. Anderoglu, A. Misra, H. Wang, F. Ronning, M. F. Hundley, and X. Zhang, Appl. Phys. Lett. **93**, 083108 (2008).
[6]X. Zhang, H. Wang, X. H. Chen, L. Lu, K. Lu, R. G. Hoagland, and A. Misra, Appl. Phys. Lett. **88**, 173116 (2006).
[7]J. Wang, O. Anderoglu, J. P. Hirth, A. Misra, and X. Zhang, Appl. Phys. Lett. **95**, 021908 (2009).
[8]J. Wang, N. Li, O. Anderoglu, X. Zhang, A. Misra, J. Y. Huang, and J. P. Hirth, Acta Mater. **58**, 2262 (2010).
[9]N. Li, J. Wang, J. Y. Huang, A. Misra, and X. Zhang, Scr. Mater. **64**, 149 (2011).
[10]L. Lu, X. Chen, X. Huang, and K. Lu, Science **323**, 607 (2009).

[11]L. Lu, Y. F. Shen, X. Chen, L. H. Qian, and K. Lu, Science **304**, 422 (2004).
[12]E. Ma, Y. M. Wang, Q. H. Lu, M. L. Sui, L. Lu, and K. Lu, Appl. Phys. Lett. **85**, 4932 (2004).
[13]X. Zhang, A. Misra, H. Wang, M. Nastasi, J. D. Embury, T. E. Mitchell, R. G. Hoagland, and J. P. Hirth, Appl. Phys. Lett. **84**, 1096 (2004).
[14]O. Anderoglu, A. Misra, H. Wang, and X. Zhang, J. Appl. Phys. **103**, 094322 (2008).
[15]C. J. Shute, B. D. Myers, S. Xie, T. W. Barbee Jr., A. M. Hodge, and J. R. Weertman, Scr. Mater. **60**, 1073 (2009).
[16]J. Wang and H. Huang, Appl. Phys. Lett. **88**, 203112 (2006).
[17]T. Zhu, J. Li, A. Samanta, H. G. Kim, and S. Suresh, Proc. Natl. Acad. Sci. USA **104**, 3031 (2007).
[18]K. A. Afanasyev and F. Sansoz, Nano Lett. **7**, 2056 (2007).
[19]Z. H. Jin, P. Gumbsch, K. Albe, E. Ma, K. Lu, H. Gleiter, and H. Hahn, Acta Mater. **56**, 1126 (2008).
[20]A. J. Cao, Y. G. Wei, and S. X. Mao, Appl. Phys. Lett. **90**, 151909 (2007).
[21]Y. B. Wang and M. L. Sui, Appl. Phys. Lett. **94**, 021909 (2009).
[22]J. A. Brown and N. M. Ghoniem, Acta Mater. **58**, 886 (2010).
[23]J. A. Brown and N. M. Ghoniem, Acta Mater. **57**, 4454 (2009).
[24]O. Anderoglu, A. Misra, J. Wang, R. G. Hoagland, J. P. Hirth, and X. Zhang, Int. J. Plasticity **26**, 875 (2010).
[25]X. Y. Li, Y. J. Wei, L. Lu, K. Lu, and H. J. Gao, Nature (London) **464**, 877 (2010).
[26]J. P. Hirth and J. Lothe, *Theory of Dislocations* (Krieger, Melbourne, FL, 1992).
[27]V. Yamakov, D. Wolf, S. R. Phillpot, and H. Gleiter, Acta Mater. **50**, 5005 (2002).
[28]J. Wang and H. Huang, Appl. Phys. Lett. **85**, 5983 (2004).
[29]R. C. Pond and L. M. F. Garcia-Garcia, *Deformation Twinning in Aluminium*, Institute of Physics Conference Series No. 61 (Institute of Physics Publishing, Bristol and Philadelphia, 1981), Chap. 10, p. 495.
[30]M. S. Daw and M. I. Baskes, Phys. Rev. B **29**, 6443 (1984).
[31]S. M. Foiles, M. I. Baskes, and M. S. Daw, Phys. Rev. B **33**, 7983 (1986).
[32]Y. Mishin, M. J. Mehl, D. A. Papaconstantopoulos, A. F. Voter, and J. D. Kress, Phys. Rev. B **63**, 224106 (2001).
[33]Y. Mishin, D. Farkas, M. J. Mehl, and D. A. Papaconstantopoulos, Phys. Rev. B **59**, 3393 (1999).
[34]H. Huang and J. Wang, Appl. Phys. Lett. **83**, 4752 (2003).
[35]J. Wang, H. Huang, and T. S. Cale, Modell. Simul. Mater. Sci. Eng. **12**, 1209 (2004).
[36]J. Wang, R. G. Hoagland, and A. Misra, Appl. Phys. Lett. **94**, 131910 (2009).
[37]J. Wang and H. Huang, Appl. Phys. Lett. **85**, 5983 (2004).
[38]J. Wang, R. G. Hoagland, and A. Misra, J. Mater. Res. **23**, 1009 (2008).
[39]J. Wang, H. Huang, S. V. Kesapragada, and D. Gall, Nano Lett. **5**, 2505 (2005).
[40]J. Wang, R. G. Hoagland, J. P. Hirth, and A. Misra, Acta Mater. **56**, 3109 (2008).
[41]J. Wang, R. G. Hoagland, J. P. Hirth, and A. Misra, Acta Mater. **56**, 5685 (2008).
[42]R. G. Hoagland, T. E. Mitchell, J. P. Hirth, and H. Kung, Philos. Mag. **82**, 643 (2002).
[43]J. W. Cahn and J. E. Taylor, Acta Mater. **52**, 4887 (2004).
[44]A. Suzuki and Y. Mishin, Mater. Sci. Forum **502**, 157 (2005).
[45]J. W. Cahn, Y. Mishin, and A. Suzuki, Acta Mater. **54**, 4953 (2006).
[46]S. G. Srinivasan and J. W. Cahn, in *Science and Technology of Interfaces*, edited by S. Ankem, C. S. Pande, I. Ovidko, and R. Ranganathan (TMS, Seattle, 2002), p. 3.
[47]D. Molodov, A. Ivanov, and G. Gottstein, Acta Mater. **55**, 1843 (2007).
[48]W. Winning, G. Gottstein, and L. S. Shvindlerman, Acta Mater. **49**, 211 (2001).
[49]W. Winning, G. Gottstein, and L. S. Shvindlerman, Acta Mater. **50**, 353 (2002).
[50]M. Winning and A. D. Rollett, Acta Mater. **53**, 2901 (2005).
[51]H. Yoshida, K. Yokoyama, N. Shibata, and Y. I. A. T. Sakuma, Acta Mater. **52**, 2349 (2004).
[52]J. P. Hirth and R. C. Pond, Acta Mater. **44**, 4749 (1996).
[53]R. C. Pond and J. P. Hirth, *Solid State Physics* (Academic, New York, 1994), vol. 47, p. 287
[54]J. Wang, R. G. Hoagland, J. P. Hirth, L. Capolungo, I. J. Beyerlein, and C. N. Tomé, Scr. Mater. **61**, 903 (2009).
[55]J. Wang, J. P. Hirth, and C. N. Tomé, Acta Mater. **57**, 5521 (2009).
[56]M. L. Kronberg, Acta Metall. **5**, 507 (1957).
[57]R. C. Pond, S. Celotto, and J. P. Hirth, Acta Mater. **51**, 5358 (2003).
[58]R. C. Pond and J. P. Hirth, Philos. Mag. **90**, 805 (2010).
[59]J. Wang, J. P. Hirth, R. C. Pond, and J. M. Howe, Acta Mater. **59**, 241 (2011).